Solar Physics
DOI: 10.1007/•••••-•••-•••-••••-•

A New Solar Imaging System for Observing High Speed Eruptions: Solar Dynamics Doppler Imager (SDDI)

Kiyoshi Ichimoto[1,2] · Takako T. Ishii[1] · Kenichi Otsuji[1] · Goichi Kimura[1] · Yoshikazu Nakatani[1] · Naoki Kaneda[1] · Shin'Ichi Nagata[1] · Satoru Ueno[1] · Kumi Hirose[1] · Denis Cabezas[1] · Satoshi Morita[2]

Abstract A new solar imaging system was installed at Hida observatory to observe the dynamics of flares and filament eruptions. The system (Solar Dynamics Doppler Imager; SDDI) takes full disk solar images with a field of view of 2520"x 2520" at multiple wavelengths around Hα line at 6562A. Regular operation was started in May 2016, in which images at 73 wavelength positions spanning from Hα−9A to Hα+9A are obtained every 15 seconds. The large dynamic range of measurement of the line-of-sight velocity (±400 km/sec) allows us to determine the real motions of erupting filaments in 3D space. It is expected that SDDI provides unprecedented data set to study the relation between kinematics of filament eruptions and Coronal Mass Ejections (CME), and contribute to the real time prediction of the occurrence of CMEs that cause a significant impact on the space environment of the earth.

Keywords: Sun, imaging system, flare, filament eruption, CME

1. Introduction

It is known that many of coronal mass ejections (CME), the primary driver of the solar storms that impact the space environment of the earth, are associated with prominence/filament eruptions, and the erupted prominence is sometimes observed as a bright core of the CME (e.g. Gopalswamy, 2015, Howard, 2015). Munro (1979) reported that 70% of CME are associated with a filament disappearance, while Gopalswamy et al. (2003) found that 72% of prominence

[1] Kwasan and Hida Observatories, Kyoto University

[2] National Astronomical Observatory of Japan

eruptions are clearly accompanied by CMEs. Morimoto and Kurokawa (2003) studied 15 events of filament disappearance and found that 8 events that were identified as eruptive one were all associated with CME and other 7 events that were identified as 'quasi-eruptive' or non-eruptive one were not associated with CME. Close relationship between kinematics of prominence eruption and CME is also known (Gopalswamy. 2015), i.e., there is a good correlation between the ascending speeds and directions of prominence eruption and CME. These facts strongly suggest that observations of erupting motions of prominence/filaments provide a valuable mean for predicting the occurrence of CME that impacts the earth.

Ascending velocities of prominence eruptions are so far mainly measured for events observed on the solar limb, for which time variation of apparent heights of erupting prominence projected on the sky were obtained from a series of images. Shimojo (2014) reported the ascending velocities of prominence eruptions observed by Nobeyama Radio Heliograph on the solar limb in July 1992 $\sim$ March 2013, and found that the yearly average of the radial velocity is about 100 km/s except the solar minimum and some of them reached 400km/sec. Similar result was reported by McCauley etal (2015) using 904 events observed by Atmospheric Imaging Assembly (AIA) aboard the Solar Dynamics Observatory (SDO). In these observations, we lack the information of the line-of-sight component of velocity of erupting prominences nor their real speed and direction in 3D space.

Line-of-sight velocities of erupting filaments, i.e., the motions towards the earth, have been rarely observed to a large traveling distance. A few exceptions are found in a spectroscopic observation from ground and a stereoscopic observation from space, both of which observed a filament eruption that took place near the central meridian of the sun seen from the earth. Penn (2000) obtained the line-of-sight velocity of 200$\sim$300km/s for an ascending filament by spectroscopic observation in HeI 10830A and determined its trajectory up to the height of 0.5 solar radii. Filippov (2013), using Solar Terrestrial Relations Observatory (STEREO) and the SDO, determined the ascending velocity of a filament eruption up to the height of 300Mm (0.43 solar radii) and found that, during the initial stage of the eruption, the filament moved along the magnetic neutral surface. It is noted that such observations are rare cases that highly rely on chance.

The lack of information of the line-of-sight velocity of filament eruptions is largely due to limited dynamic range of Doppler measurement in synoptic Hα observations of current ground-based facilities. Many observatories conduct synoptic solar observations in Hα with a passband width of 0.25$\sim$0.5A and a fixed wavelength at the line center. At some solar observing stations, off-band Hα images are also taken in regular basis, but their ranges in wavelength offset are insufficient to capture the Doppler shift of high speed eruptions; for examples, they are $\pm$0.8A for Flare Monitoring Telescope (FMT, Kurokawa et al 1995) that was/are in operational at Hida observatory (1992-2009) and Ica University in Peru (2010 -), $\pm$1.2A for Solar Magnetic Activity Research Telescope (SMART; Ueno et al. 2004, the former system of the present one reported in this paper) at Hida observatory, and $\pm$0.5A at Fuxian Lake Observatory (ONSET; Fang et al 2013). Thus filament eruptions with a line-of-sight velocity grater than about

60km/s erude observers and we are almost blind to such high speed eruptions moving toward the earth with the current observing facilities.

To open a new eye for watching the high speed motions of filament eruptions and to investigate the way for predicting the occurrence of geo-effective CMEs, we developed a new Hα imaging system that covers a wide range of wavelength around Hα under the Project for Solar-Telestrial Environment Prediction (PSTEP: http://www.pstep.jp/?lang=en). The new system, Solar Dynamics Doppler Imager (SDDI), started the regular operation at Hida observatory in May 2016. In this paper, we describe the basic features of SDDI and demonstrate its performance with some initial data.

2. Observing system

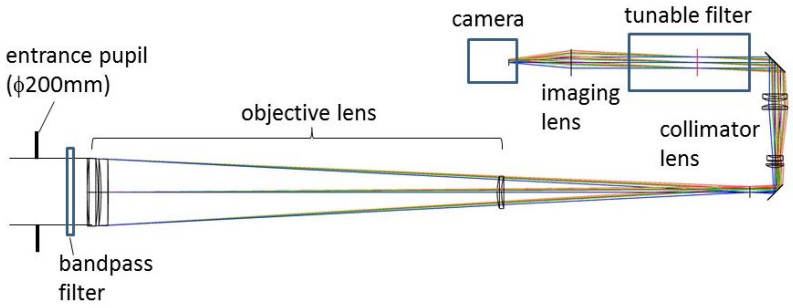

Figure 1. Optical layout of SDDI

The imaging system was installed on an optical bench of one of four telescopes of the SMART at Hida Observatory of Kyoto University. Optical layout is shown in Figure 1. The system consists of a refracting telescope with an aperture diameter of 20 cm, a tunable Lyot filter, a high speed CMOS camera with 2k×2k pixels and feeding optics. At the entrance of the telescope, a bandpass filter that transmits lights in a wavelength range of 6300∼7000A is placed to reduce the heat load into the system. The design of the imaging optics is optimized for the Hα wavelength and it has nearly diffraction limited image quality in Hα over the field of view covering the full solar disk. After the primary focus of the objective lens (f=4000 mm), a lens unit collimates the beam to form a pupil image with a diameter of 33mm at the center of the tunable Lyot filter. Finally the reimaging lens with a focal length of 170 mm forms a solar image on the camera with a plate scale of 190 arcsec/mm. The spatial sampling is 1.23 arcsec/pix and the field of view (FOV) covered by the camera is 2520 × 2520 arcsec, while there is some vignetting of lights by the tunable filter at the corners of the FOV. The camera is mounted on a linear stage and translated remotely along the optical axis for adjusting the focus. Since the diffraction limited resolution of a 20cm telescope at 6563A is 0.83 arcsec, the spatial sampling of the system is not sufficiently high. This is because we prioritize the field coverage and time resolution rather than the spatial resolution by considering the scientific objective of the SDDI.

Table 1. Basic properties of SDDI

Optical system	
Telescope diameter	200 mm
Effective focal length	1086 mm
Beam at tunable filter	Collimated with a ϕ33mm pupil
Tunable filter	
Passband width (FWHM)	0.25A
Aperture	40 × 40 mm
Tuning range	H$\alpha\pm$9A
Response time	$<$ 0.1 sec
Peak transmission	4.8 %
Camera: Hamamatsu Photonics Co. ORCA Flash 4.0	
Format	2048 × 2048 pixels
Pixel size	6.5 μm
Data depth	16 bits
Frame rate	100 frames/sec (max.)
System	
Field of view	2520" × 2520"
Spatial sampling	1.23 arcsec/pixel
Exposure time	2 msec (typical)
Time cadence	15 sec for 73 wavelengths (typical)
Dynamic range of LOS velocity	$-400 \sim +400$ km/s

Upgrading the camera with a larger format one is, however, one of the desired improvement of the system in future. The basic parameters of the SDDI system are summarized in Table 1.

The tunable filter is a conventional Lyot type birefringent filter consisting of 7 stage calcite blocks with an aperture of 40 mm×40 mm. The bandpass width (FWHM) and the free spectral range at Hα are 0.25A and 32A, respectively. In each block, a nematic type Liquid Crystal Variable Retarders (LCVR, products of Meadowlark Optics) is equipped, and by applying specific voltages on each LCVR, we can set the wavelength of the peak transmission at any wavelength in the range of H$\alpha\pm$9A with a response time shorter than 0.1 sec. The peak transmission is 4.8% and the wavefront error is 61nm (rms) after removal of tilt and power components. Figure 2 shows the transmission profiles of the tunable filter and blocking filter together with the solar spectrum around Hα line. The scheme for controlling the LCVR voltages to tune the wavelength is based on the heritage from the formerly developed universal tunable filter at Hida observatory (Hagino etal 2013).

Figure 3 shows the block diagram of the controlling system. The tunable filter and the camera are controlled through USB and Camera-link interfaces, respectively, by on-board PC (Windows10) that is mounted on the optical bench of the telescope. The observing software is written by Visual-C and Interactive Data Language (IDL) on the on-board PC, and is manipulated from the operation PC

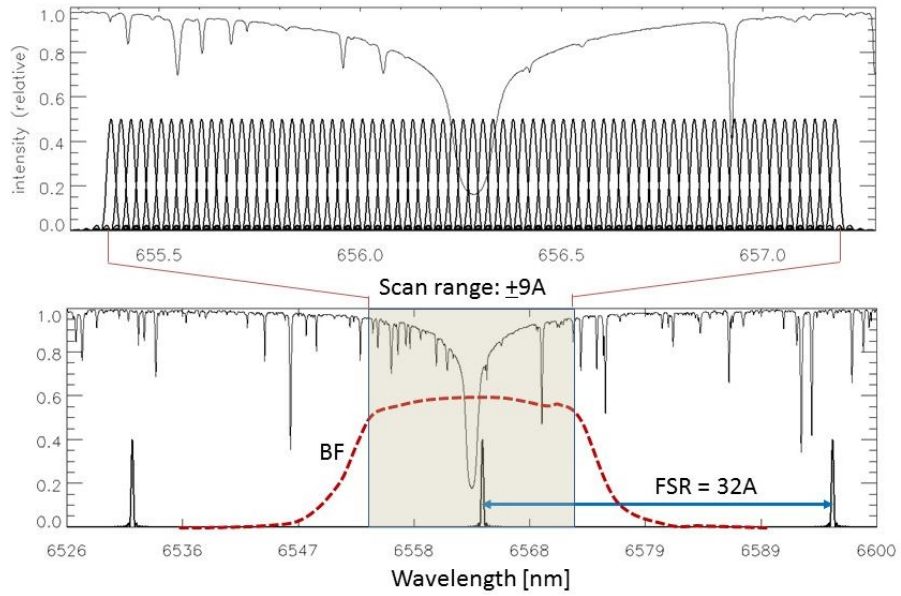

Figure 2. Transmission profiles of tunable filter (thick line) and blocking filter (dashed line) together with the solar spectrum (solid line).

located in the observing room through the ethernet. The image data obtained by the camera are directory stored in SSD or hard disks on the operation PC.

More details of characteristics of the instrument will be described in a separate paper.

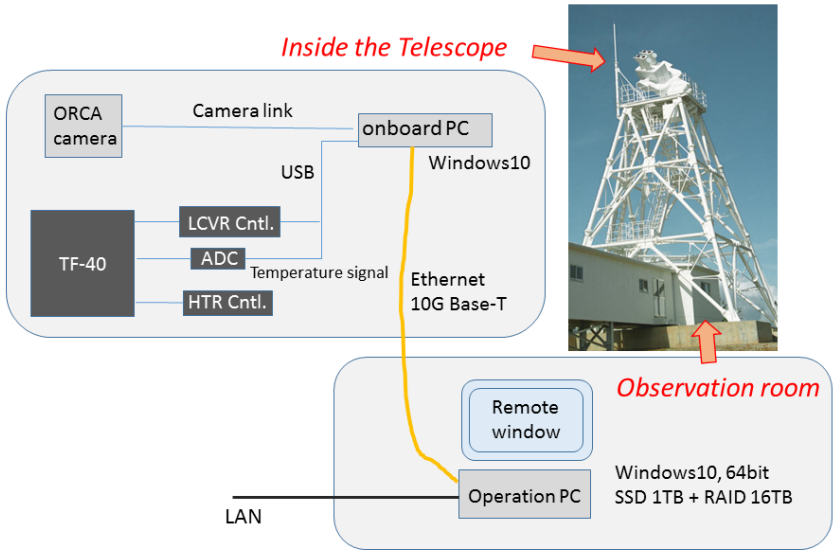

Figure 3. Block diagram of the observing system.

3. Operation and data archive

The system was installed on SMART at the end of April 2016 after extensive characterization of the tunable filter with a spectrometer of the Domeless Solar Telescope at Hida observatory. Regular operation of the system was then started from the beginning of May. The standard sequence of data acquisition in daily observations is to take full field images at 73 wavelength positions spanning from −9A to +9A with a constant wavelength step of 0.25A. With a typical exposure time of 2msec, a set of images can be obtained in 15 sec (In initial phase of the operation until the end of July 2016, number of wavelength positions were 61 or 41 in a range from −8A to +8A and time cadence were 30 or 20 sec, respectively.) . Quick look images are processed by the operation PC in real time and are opened to the internet at the web site http://www.hida.kyoto-u.ac.jp/SMART/live/index2.html (see Figure 4).

10 hour observation in a day thus produces data of about 1.4TB. To reduce the total amount of data to be stored, we discard images in continuum, i.e., images with the wavelength offset larger than ±3A, unless high speed event is detected in sum images in $-5A \sim -4$A and $+4 \sim +5$A from Hα center. Quick look and selected data are accessible on the web site at http://www.hida.kyoto-u.ac.jp/SMART/ .

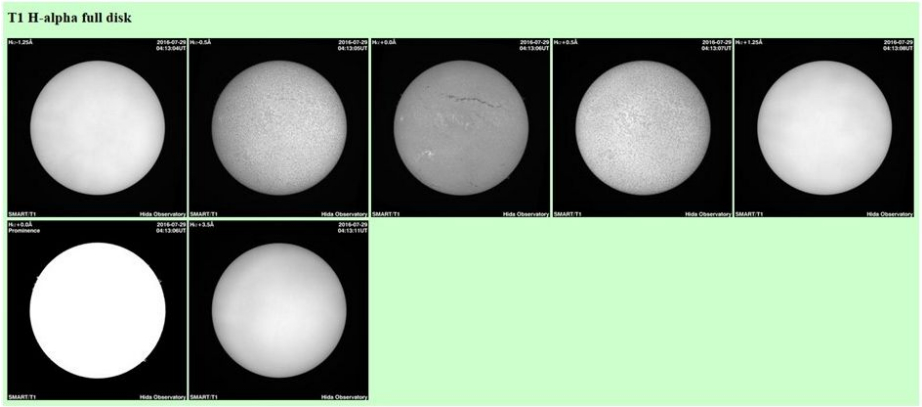

Figure 4. Live images of SDDI for real time distribution of observing status.

In raw images, we recognized fringe patterns that vary with the wavelength. The contrast and spatial scale of the pattern are a few percent in intensity and several arc minutes, respectively. This is not a serious problem for inspection of images to search interesting active events and morphological studies of eruptive phenomena. However correction of such artificial patterns is demanded for quantitative studies using spectral profiles. To remove the fringe pattern, we apply gain correction using 'flat' images constructed for each 73 wavelength by using the Kuhn-Lin-Loranz method (Kuhn et al , 1991). Figure 5 shows an example of flat image taken at Hα−1A and a 'Dopplergram' made from the subtraction of flat images at Hα−0.5A and Hα+0,5A divided by the the sum of them. It is noticed that the 'Dopplergram' shows apparent blue shift towards the outer

part of the field of view. This is because the gradual red shift of the transmission peak of the Lyot filter due to the increasing incidence angle of the collimated light to the filter towards the outer part of the field of view. The amount of the wavelength shift is approximately 0.11, 0.19 and 0.38A at the solar limb (920 arcsec from the center of FOV), edge (1260 arcsec) and corner (1782 arcsec) of the FOV, respectively.

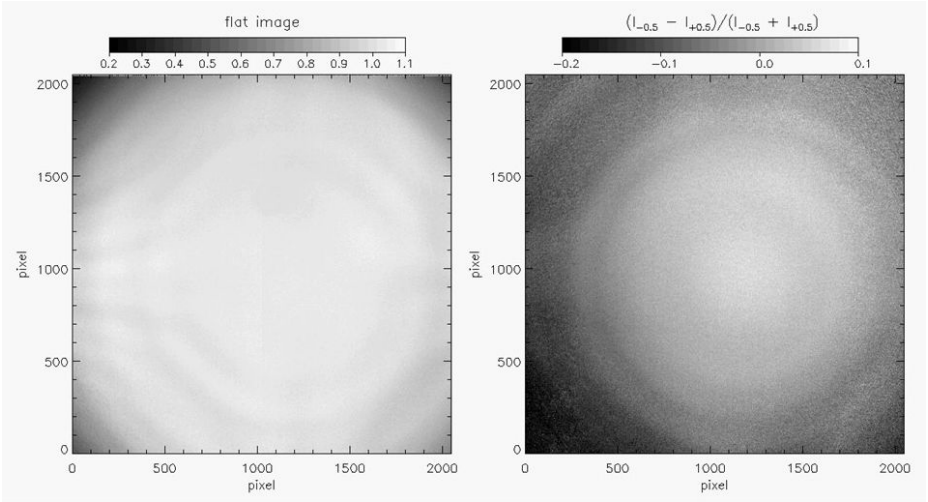

Figure 5. An example of flat image taken at H$\alpha-1$A (right) and a 'Dopplergram' made from the flat images at H$\alpha-0.5$A and H$\alpha+0{,}5$A. The flat image is normalized by its median value and displayed with a range from 0.2 to 1.1.

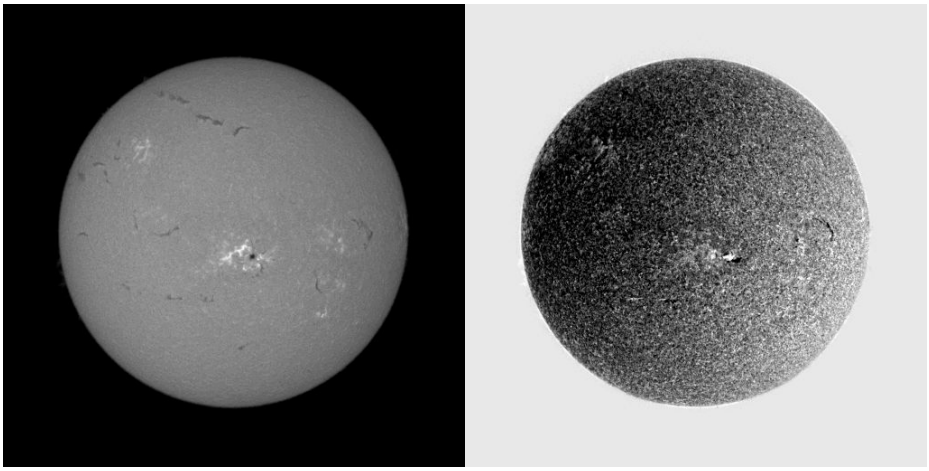

Figure 6. An example of SDDI image taken at Hα center (left) and difference image of H$\alpha\pm0.5$A (right). Top is the geographical north and left is the east

4. Initial data

Figure 6 shows an example of raw image in Hα line center and accompanied Dopplergram made from the difference of two images in H$\alpha\pm$0.5A. In the display, the flat field correction was not applied for Hα intensity image, while for the Dopplaergram, flat field collection was applied to both $\pm$0.5A images since without the flat correction, artificial patterns are obvious in the Dopplergram. Solar rotation and local flow patterns are clearly recognized, while global variation of Doppler signal need to be taken with a care because of gradual shift of wavelength of the transmission peak of the Lyot filter as noted above.

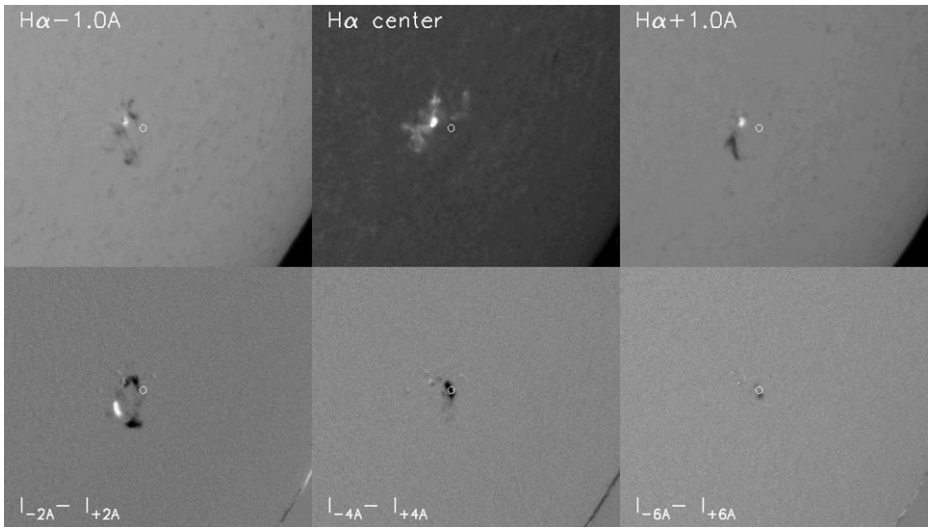

Figure 7. C class flare and filament eruption on 7 July 2016 07:55:49UT occurred in NOAA 12561. Top is the geographical north and left is the east

On 7th July, we observed a compact C class flare and associated filament eruption in NOAA 12561. Figure 7 shows images in Hα center and H$\alpha\pm$1.0A, and difference images of H$\alpha\pm$2A, H$\alpha\pm$4A, and H$\alpha\pm$6A, while the spectral profile of ascending part of the erupting filament marked by circles is shown in Figure 8 together with a spectrum in normal region. It is noted that the profiles shown in Figure 8 is convolutions of the real solar spectra and the filter transmission curve. Though this observation was conducted with 41 wavelength positions spanning from Hα-8A to Hα+8A, it clearly demonstrates the necessity of wide range of wavelength coverage to capture dynamic eruptions, i.e., the absorption feature of the ascending blob is clearly recognized only in images with a wavelength offset larger the -2A.

5. Summary and Prospects

A new solar synoptic observation system, SDDI, was successfully installed on SMART at Hida observatory and is conducting regular operation since the beginning of May 2016. SDDI observes the motion of filament/prominence eruptions

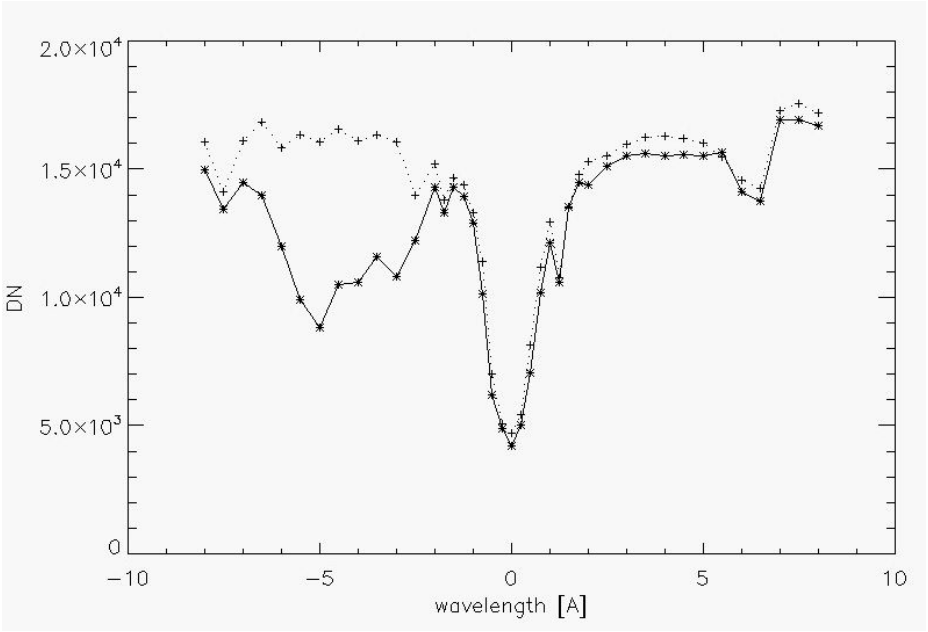

Figure 8. Spectral profiles of the eruption (solid line) and disk center (dotted line) after flat field correction.

with a line of sight velocity of up to ∼400 km/s, and enable us to capture the real motions of large scale high speed eruptions in 3D space for the first time with a wide field of view (2520×2520 arcsec) and a high time cadence (15 sec). Increasing the spatial sampling with a larger format camera can be a subject for future improvement of the system to utilize the full optical performance.

It is expected that the data obtained by SDDI will provide a new methodology of the space weather forecasting by relating the kinematic properties of filament/prominence eruptions and the occurrence of CME that reaches the earth. Identifying the activation of filament prior to its sudden destabilization will also contribute to the prediction of its occurrence and understanding of the onset mechanism of filament eruption. Moreover the three dimensional velocity field of erupting filaments and its time evolution informs us the spatial distribution of accelerating force acting on prominence plasma, and provide crucial information for understanding the acceleration mechanism of the filament. The data is available on the web site of the Hida observatory.

Acknowledgments The authors are grateful to the staff of Hida observatory for supporting the instrument development and daily observations. This work was supported by MEXT/JSPS KAKENHI Grant Number JP15H05814, Project for Solar-Terrestrial Environment Prediction (PSTEP).

References

Fang, C., Chen, P.-F., Li, Z., et al. 2013, *Research in Astronomy and Astrophysics*, 13, 1509-1517

Filippov, B. 2013, *Astrophys. J.*, 773, 10
Gopalswamy, N., Shimojo, M., Lu, W., et al. 2003, *Astrophys. J.*, 586, 562
Gopalswamy, N. 2015, Solar Prominences, 415, 381
Hagino, M., Ichimoto, K., Kimura, G., et al. 2014, *Proc. SPIE*, 9151, 91515V
Howard, T. A. 2015, *Astrophys. J.*, 806, 175
Kuhn, J.R., Lin, H. and Loranz, D. 1991, PASP, 103, 1097
Kurokawa, H., Ishiura, K., Kimura, G., Nakai, Y., Kitai, R., Funakoshi, Y., and Shinkawa, T. 1995, *J. Geomag. Geoelectr.*, 47, 1043
McCauley, P. I., Su, Y. N., Schanche, N., et al. 2015, *Solar Phys.*, 290, 1703
Morimoto, T., & Kurokawa, H. 2003, *Pub. Astron. Soc. Japan*, 55, 1141
Munro, R. H., Gosling, J. T., Hildner, E., et al. 1979, *Solar Phys.*, 61, 201
Penn, M. J. 2000, *Solar Phys.*, 197, 313
Shimojo, M. 2014, Nature of Prominences and their Role in Space Weather, 300, 161
UeNo, S., Nagata, S.-i., Kitai, R., Kurokawa, H., & Ichimoto, K. 2004, proc. SPIE, 5492, 958